Phase stability and B-site ordering in La_2NiMnO_6 thin films

Xiao-Wei Jin, Lu Lu, Shao-Bo Mi' , Ming Liu, and Chun-Lin Jia

Citation: Appl. Phys. Lett. **109**, 031904 (2016); doi: 10.1063/1.4959242
View online: http://dx.doi.org/10.1063/1.4959242
View Table of Contents: http://aip.scitation.org/toc/apl/109/3
Published by the American Institute of Physics

Phase stability and B-site ordering in La_2NiMnO_6 thin films

Xiao-Wei Jin,[1] Lu Lu,[1] Shao-Bo Mi,[2,a)] Ming Liu,[1] and Chun-Lin Jia[1,2,3]
[1]*The School of Electronic and Information Engineering, Xi'an Jiaotong University, Xi'an 710049, People's Republic of China*
[2]*State Key Laboratory for Mechanical Behavior of Materials, Xi'an Jiaotong University, Xi'an 710049, People's Republic of China*
[3]*Peter Grünberg Institute and Ernst Ruska Center for Microscopy and Spectroscopy with Electrons, Forschungszentrum Jülich, D-52425 Jülich, Germany*

(Received 25 May 2016; accepted 8 July 2016; published online 20 July 2016)

Thin films of multiferroic double-perovskite La_2NiMnO_6 are prepared on (001)-oriented $SrTiO_3$, $(La_{0.289}Sr_{0.712})(Al_{0.633}Ta_{0.356})O_3$, and $LaSrAlO_4$ substrates by pulsed laser deposition. Microstructure investigation by advanced electron microscopy shows that the La_2NiMnO_6 films have a monoclinic structure on the $SrTiO_3$ substrates and a rhombohedral structure on the $(La_{0.289}Sr_{0.712})(Al_{0.633}Ta_{0.356})O_3$ and $LaSrAlO_4$ substrates. Atomic-scale elemental maps of the monoclinic and rhombohedral phases reveal a short-range and/or partial ordering of the B-sites. In addition, domains and columnar grains are found in the films. Our results demonstrate that the phase and microstructure of the La_2NiMnO_6 films can be tuned by epitaxial strains induced by different substrates. *Published by AIP Publishing.*
[http://dx.doi.org/10.1063/1.4959242]

With its high paramagnetic-to-ferromagnetic Curie temperature (~280 K) and good magnetic properties near room temperature, the multiferroic (ferroelectric and ferromagnetic) double-perovskite La_2NiMnO_6 (LNMO) has been considered as a promising candidate of ferromagnetic semiconductor for magnetoelectronics and spintronics, and thus attracted much research attention in recent decades.[1–4] The crystallographic ordering and oxidation states of the B-site cations (Ni and Mn) in LNMO related to the nature of the ferromagnetism have been extensively studied by various analytical techniques, such as nuclear magnetic resonance (NMR) spectroscopy,[5] X-ray photoelectron spectroscopy,[6] X-ray absorption spectroscopy,[7] and neutron scattering.[2,8] Mn^{4+}/Ni^{2+} oxidation states have been detected in the B-site ordered LNMO phase with a Curie temperature of 280 K.[4] Mn^{3+}/Ni^{3+} and Mn^{4+}/Ni^{2+} were found to coexist in the B-site disordered LNMO phase with a Curie temperature of 150 K.[9,10]

In the case of a phase mixture material of B-site ordered and disordered LNMO, two Curie temperatures of 280 K and 150 K have been observed.[11] In the ordered structure, $Mn^{4+}-O^{2-}-Ni^{2+}$ superexchange interaction is believed to give rise to the magnetic properties of LNMO.[2,4] In addition, the crystal structure of the LNMO compound has been investigated by means of X-ray diffraction, neutron diffraction, and polarized Raman spectra.[2,8,12] It was found that LNMO is rhombohedral ($R\bar{3}$ or $R\bar{3}c$) at high temperature, which transforms to monoclinic ($P2_1/n$) or orthorhombic (Pbnm) at low temperature.[13] The coexistence of rhombohedral and monoclinic/orthorhombic phase was observed in LNMO at room temperature.[1,4,14] Moreover, rhombohedral LNMO ($R\bar{3}$) and monoclinic LNMO ($P2_1/n$) are partially B-site-ordered;[15–17] rhombohedral LNMO ($R\bar{3}c$) and orthorhombic LNMO (Pbnm) are completely B-site-disordered.[14,18]

To fulfill the demands for integrated devices, epitaxial thin films of LNMO have been fabricated on different substrates by pulsed laser deposition (PLD).[10,12,13,18–24] It is known that the microstructure and physical properties of thin films can be influenced by many factors, e.g., the growth conditions including growth temperature and oxygen pressure, and the epitaxial strain induced by the film-substrate lattice mismatch.[3,22,25,26] For instance, the phase stability and the related physical properties of the $BiFeO_3$ films were strongly affected by the epitaxial strain. $BiFeO_3$ films grown on $YAlO_3$ illustrate a tetragonal-like phase, while the films fabricated on $SrTiO_3$ (STO) and $DyScO_3$ are a rhombohedral-like phase.[27] In comparison with the extensive studies on the synthesis and properties of bulk LNMO, investigations on LNMO thin films are still limited. In this letter, the microstructures of LNMO thin films grown on different substrates, (001)-oriented $SrTiO_3$ (STO), $(La_{0.289}Sr_{0.712})(Al_{0.633}Ta_{0.356})O_3$ (LSAT), and $LaSrAlO_4$ (LSAO), are systematically investigated. In particular, the ordering of B-sites of the LNMO thin films is studied on atomic scale by means of advanced electron microscopy. The effects of epitaxial strain on phase stability and domain structure of the LNMO thin films are discussed based on the obtained results.

The LNMO thin films were deposited on (001)-oriented STO, LSAT, and LSAO substrates by the PLD technique. A KrF excimer laser (wavelength 248 nm) was used for ablation of a sintered La_2NiMnO_6 target. For the film preparation on different substrates, the same conditions were used, including the substrate temperature (800 °C), oxygen pressure (250 mTorr), target-substrate distance (10 cm), laser fluence (2 J/cm^2), and repetition frequency (5 Hz). Cross-sectional transmission electron microscopy (TEM) samples were prepared by focused ion beam (FIB) technique. Bright-field (BF) TEM images and selected area electron diffraction (SAED) patterns were acquired by a JEM 2100 TEM. Atomic-resolution high-angle annular dark field (HAADF) imaging

a)Author to whom correspondence should be addressed. Electronic mail: shaobo.mi@xjtu.edu.cn

and energy-dispersive X-ray spectroscopy (EDS) mapping were performed on a JEOL ARM200F microscope with a probe aberration corrector, operated at 200 kV.

Figure 1(a) shows a low-magnification BF-TEM image of the LNMO/STO(001) heterosystem recorded along the [100] zone axis of STO. The interface between the films and the substrates is denoted by a horizontal arrow. No interfacial dislocations are observed at the film-substrate interface. In comparison with the substrate, the contrast variation within the films can be detected, which divides the films into several sub-regions, e.g., O_1, O_2, and O_3. The SAED pattern taken from the region O_1 and O_3 is displayed in Figures 1(b) and 1(d), respectively. Figure 1(c) displays the SAED pattern of the region including O_1 and O_2 as illustrated by a broken-line circle in Figure 1(a). In contrast to Figure 1(b), additional diffraction spots belonging to the region O_2 can be detected, as demonstrated by a vertical arrow in Figure 1(c). According to the experimental results, the LNMO films may have either an orthorhombic or a monoclinic phase[14,15] since orthorhombic and monoclinic LNMO cannot be easily distinguished from each other only by the SAED. Regarding the SAED patterns, the orientation relationships between the films and the substrates in the region of O_1, O_2, and O_3 can be described as $[110](001)_{LNMO}//[100](001)_{STO}$, $[1\bar{1}0](110)_{LNMO}//[100](001)_{STO}$, and $[001](110)_{LNMO}//[100](001)_{STO}$, respectively, resulting in three different domains. Figure 1(e) shows schematically the relations of the three domains of the LNMO films with the STO(001) substrates. Therefore, the contrast variation in the LNMO films in Figure 1(a) results from the existence of oriented domains in the films. It is noted that the domain boundaries in the LNMO films start from the film-substrate interface and penetrate the whole film.

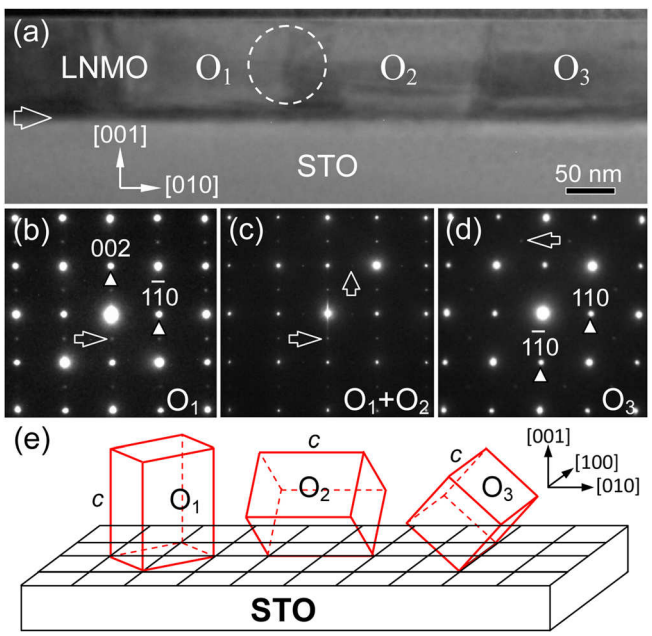

FIG. 1. (a) A low-magnification BF-TEM image of a LNMO film on STO(001) substrate viewed along the [100] zone axis of the substrates. A horizontal arrow denotes the film-substrate interface. O_1, O_2, and O_3 mark three different regions of the films. A broken-line circle denotes a film region including O_1 and O_2. (b)–(d) The SAED patterns from the region O_1 (b), the region O_1 and O_2 (c), and the region O_3 (d), recorded along the [100] zone axis of STO. In (c), a typical diffraction peak belonging to the region O_1 and O_2 is indicated by a horizontal arrow and a vertical arrow, respectively. (e) A schematic showing the film-substrate orientation relationship at the region O_1, O_2, and O_3.

Figure 2(a) illustrates a low-magnification BF-TEM image of the LNMO/LSAT(001) heterostructure viewed along the [100] zone axis of LSAT. The film-substrate interface is denoted by a horizontal arrow. Oriented domains occur within the films, which leads to the contrast variation in the films. Along this viewing direction, the domain boundaries are mainly perpendicular to the substrates and penetrate the whole film. The width of the domains is in the range of ~10−30 nm. In addition, the domain boundaries in the film plane are observed, as marked by a vertical arrow. Figures 2(b) and 2(c) display the SAED pattern of the LNMO/LSAT heterostructure and the LNMO films containing domains recorded along the [100] zone axis of LSAT, respectively. In Figure 2(b), the diffraction spots of the LNMO film overlap with those of LSAT, which has cubic perovskite structure with a lattice parameter of a = 0.3868 nm.[26] No splitting of diffraction spots from LNMO and LSAT is observed due to very slight difference in their lattice parameters. The crystal structure of the LNMO films on LSAT is rhombohedral (to

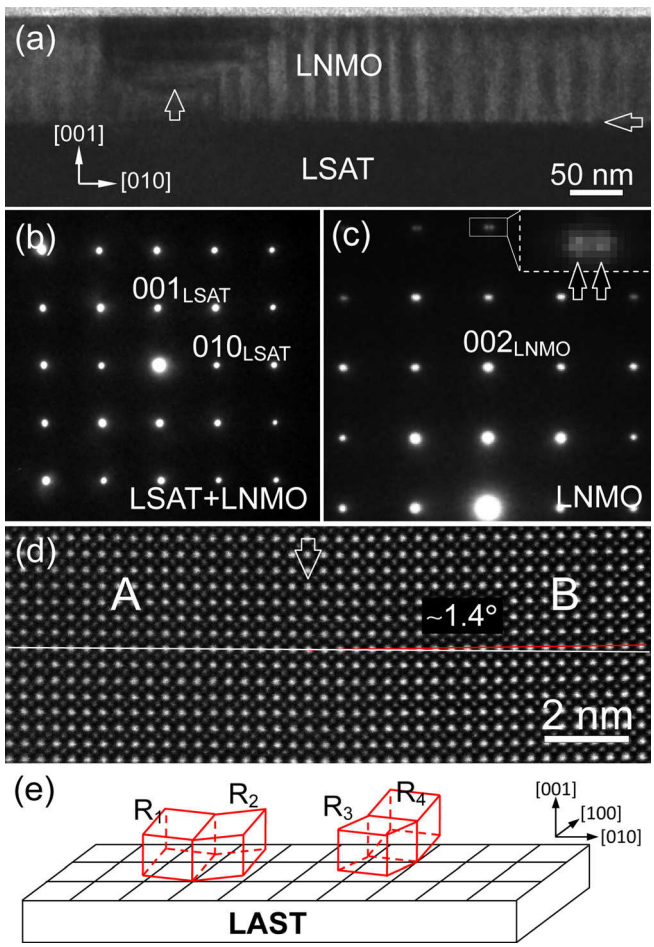

FIG. 2. (a) A low-magnification BF-TEM image of a LNMO film on LSAT(001) substrate, viewed along the [100] zone axis of the substrates. A horizontal arrow indicates the film-substrate interface. A vertical arrow denotes the domain boundaries parallel to the LSAT surface. (b) A SAED pattern of the interface area viewed along the [100] axis of LSAT. (c) A SAED pattern of the films containing oriented LNMO domains. The splitting of the diffraction spots in (c) is magnified and indicated by a pair of vertical arrows. (d) An atomic-resolution HAADF image of a part of the LNMO films including a domain boundary, recorded along the $[100]_p$ zone axis of LNMO. A vertical arrow indicates the domain boundaries. The angle between the in-plane lattice planes of the joint domains is measured as ~1.4°. (e) A schematic model of the pseudo-cubic LNMO on the LSAT(001) substrates.

simplify the following description, the rhombohedral LNMO will be treated as a pseudo-cubic perovskite lattice). In Figure 2(c), the splitting of diffraction spots can be observed for the high-index reflection spots, as denoted by a pair of vertical arrows. Figure 2(d) shows a high-resolution HAADF image of the LNMO film part containing two domains, domain A and domain B, recorded along the [100] axis of LNMO. Under the HAADF conditions, the brighter dots are La atomic columns and others are (Ni/Mn)O atomic columns. The oriented domain boundaries are indicated by a vertical arrow, where the lateral lattice planes have a misorientation angle of ~1.4° between domain A and domain B, which is consistent with the SAED results in Figure 2(c). Figure 2(e) illustrates a schematic model of the orientation relationships between the LNMO films and the LSAT substrates. It can be seen that the LNMO films have four orientations (R_1, R_2, R_3, and R_4) with the substrates. In fact, the rhombohedral distortion of the LNMO structure results in the misorientation angle of ~1.4° between two joint domains, e.g., R_1 and R_2.[14]

In addition, LSAO with larger in-plane lattice mismatch (3.009%) with LNMO was selected as substrate material to examine the phase stability and the oriented domains in LNMO. Figure 3(a) shows a low-magnification BF-TEM image, and the corresponding SAED pattern of the LNMO/LSAO(001) heterostructure viewed along the [100] zone axis of the substrates. In the SAED pattern, two sets of diffraction spots resulting from LSAO and LNMO are denoted by a red and a white rectangle, respectively. The SAED pattern shows that the LNMO film has also a rhombohedral structure. The in-plane splitting of the diffraction spots of LNMO and LSAO is visible, as demonstrated by a horizontal white arrow and a horizontal red arrow, indicating relaxation of misfit strain. Figure 3(b) shows a high-resolution HAADF image of the LNMO/LSAO(001) heterostructure, recorded along the [100] zone axis of LSAO. Misfit dislocations are detected at the film-substrate interface, as denoted by vertical white arrows. It is notable that there is a relative displacement of $a/2[001]$ (a is the parameter of pseudocubic LNMO) between the neighboring LNMO grains. The grain boundaries have a blurred contrast due to the overlap between the two LNMO grains, as indicated by a vertical red arrow. The larger lattice misfit between LNMO and LSAO and surface steps of the LSAO substrates result in the columnar growth of the rhombohedral LNMO and the formation of misfit dislocation at the interface.

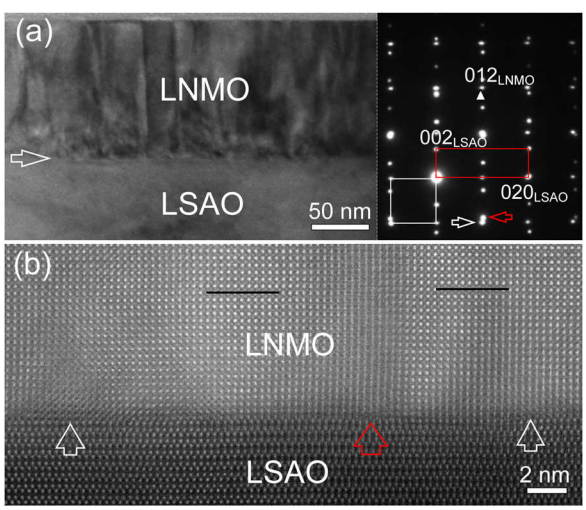

FIG. 3. (a) A low-magnification BF-TEM image of a LNMO film on LSAO(001) substrate recorded along the [100] zone axis of the substrates. A horizontal arrow denotes the LNMO/LSAO interface. The corresponding SAED pattern of the heterosystem is inserted. In the SAED pattern, the unit cells of LSAO and LNMO in the reciprocal space are indicated by a red rectangle and a white one, respectively. Horizontal arrows indicate the splitting diffraction spots of LSAO and LNMO. (b) A high-resolution HAADF image of LNMO/LSAO heterostructure viewed along the [100] zone axis of LSAO. A vertical red arrow denotes a boundary of columnar grains and vertical white arrows indicate dislocations near the film-substrate interface. Black lines denote the LaO planes of two columnar grains, which have a relative displacement of $a/2[001]$.

The disorder and order of the B-site cations (Ni and Mn) can be distinguished in the ⟨110⟩ directions of LNMO with double-perovskite structure, as schematically illustrated in Figures 4(a) and 4(b), respectively. Atomic-resolution EDS mapping has been applied to the LNMO films in order to test the ordering of the B-site cations. Figure 4(c) shows an atomic-resolution HAADF image of a LNMO film on STO, recorded along the [110] zone axis of the pseudocubic LNMO. The brighter dots are LaO atomic columns and others are Ni/Mn atomic columns. The O atomic columns cannot be detected due to the low nuclear charge values. The corresponding EDS maps for Mn and Ni are displayed in Figures 4(d) and 4(e), respectively. From the element maps, the order and disorder of the B-site cations coexist in the film, as demonstrated by red arrows and white arrows, respectively. It is noted that the partial ordering of B-site cations has been reported for the monoclinic phase of LNMO,[15,17] while the orthorhombic phase of LNMO is B-site disordered.[14] Combining the electron diffraction analysis with the EDS map, it can be concluded that under our LNMO film-growth conditions, the monoclinic phase of LNMO is obtained on the STO(001) substrate.

Moreover, the ordering of B-site cations in the LNMO films on LSAT is investigated by atomic-resolution EDS mapping. The results are shown in Figures 4(f)–4(h). In

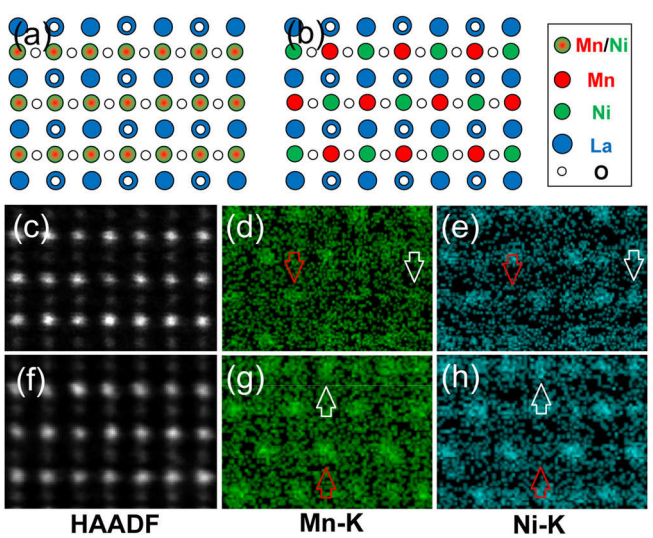

FIG. 4. A schematic model of (a) B-site-disordered and (b) B-site-ordered structure, viewed along the $[110]_P$ zone axis of LNMO. (c) Atomic-resolution HAADF image of the LNMO films on STO and corresponding EDS maps of (d) Mn and (e) Ni. (f) Atomic-resolution HAADF image of the LNMO films on LSAT and corresponding EDS maps of (g) Mn and (h) Ni.

Figures 4(g) and 4(h), both ordered and disordered B-sites can be found, as indicated by red arrows (order of B-sites) and white arrows (disorder of B-sites). In other words, the rhombohedral phase of the LNMO film has short-range ordering of the B-sites, instead of long-range ordering under our film-growth conditions, which is consistent with the reported results.[18]

Phase stability of the bulk LNMO can be modulated by different synthesis conditions.[14,15] In our case, the LNMO films were prepared under the same film-growth conditions. The different crystal structure of the LNMO films determined by TEM experiments can be attributed to the different lattice parameters and structures of the two substrates, which have mismatch with those of the film. The substrates used in our studies have perovskite or perovskite-based structure. In the surface plane of these substrates connecting the films, the in-plane structure is almost the same. Therefore, the lattice parameters become the critical factor, which lead to different levels of lattice mismatch and introduce strain into the film lattices. In the case of the monoclinic phase of LNMO on STO substrates, the lattice mismatch $(a_f - a_s)/a_s * 100\%$ (a_f, the lattice parameter of pseudocubic LNMO film and a_s, the lattice parameter of the STO substrate) is -0.794%, and thus the LNMO films are under tensile strain. For the rhombohedral phase of LNMO on the LSAT and the LSAO substrates, the lattice mismatch is 0.026% and 3.009%, respectively. The films of the rhombohedral LNMO phase are under compressive strain. The present experimental results demonstrate that a tensile strain favors formation of the monoclinic phase of LNMO, and a compressive strain facilitates the rhombohedral phase of LNMO under the used conditions for film growth. The epitaxial strain shrinks or expands the in-plane lattices of the LNMO thin films, which may not only stabilize a phase but also induce novel properties differing from a strain-free bulk counterpart, e.g., ferroelectricity in $La_2NiMnO_6/SrTiO_3$ heterostructures.[28]

Based on the atomic-resolution EDS data, the ordering of the Mn and Ni cations at B-sites is quantitatively analyzed, leading to ~91.4% of the B-sites in ordering for the monoclinic phase and ~87.8% for the rhombohedral phase. In other words, in the LNMO films of both monoclinic and rhombohedral phases, short-range and/or partial ordering occurs at the B-sites, which is independent of substrate and lattice mismatch. This suggests that the B-site ordering may be mainly controlled by the film-growth conditions, e.g., temperature and oxygen pressure.[18] Post-growth annealing of the films has been shown to enhance the B-site ordering and thus improve the performance of the materials, e.g., ferromagnetism.[29] In the LNMO/STO(001) and the LNMO/LSAT(001) heterostructures, oriented domains appear in both monoclinic and rhombohedral phases of the LNMO films, and no misfit dislocations are observed. The domain structure in the LNMO films may partially relax the lattice misfit strain in these heterostructures. In addition, the coherent domain boundaries, e.g., in the LNMO/LSAT(001), may have different crystallographic lattice symmetries from the domains, which could modify the local physical properties of the LNMO films.

In summary, the phase and B-site ordering of the LNMO films have been studied by aberration-corrected electron microscopy. It is found that the phase stability of LNMO can be modified by the epitaxial strain induced by the substrates. Under tensile strain, the monoclinic phase of the LNMO films is on the STO(001) substrates, while under compressive strain the rhombohedral phase of the LNMO films is on the LSAT(001) and LSAO(001) substrates. In addition, oriented domains and columnar grains are found in the films, depending on the lattice mismatch between the film and the substrates. The short-range and/or partial ordering of the B-sites in the films of both monoclinic and rhombohedral phases is determined by atomic-resolution EDS mapping. Our results demonstrate that the substrate-based interface engineering provides a way to control the phase formation in the LNMO films and thus modify the properties of the films.

The work was supported by the National Basic Research Program of China (No. 2015CB654903) and the National Natural Science Foundation of China (Nos. 51471169 and 51390472).

[1]J. B. Goodenough, A. Wold, R. J. Arnott, and N. Menyuk, Phys. Rev. **124**, 373 (1961).
[2]N. S. Rogado, J. Li, A. W. Sleight, and M. A. Subramanian, Adv. Mater. **17**, 2225 (2005).
[3]H. Guo, J. Burgess, S. Street, A. Gupta, T. G. Calvarese, and M. A. Subramanian, Appl. Phys. Lett. **89**, 022509 (2006).
[4]R. I. Dass, J. Q. Yan, and J. B. Goodenough, Phys. Rev. B **68**, 064415 (2003).
[5]A. Kichizo, S. Hisashi, and I. Shuichi, J. Phys. Soc. Jpn. **47**, 1054 (1979).
[6]V. L. Joseph Joly, P. A. Joy, S. K. Date, and C. S. Gopinath, Phys. Rev. B **65**, 184416 (2002).
[7]M. C. Sánchez, J. García, J. Blasco, G. Subías, and J. Perez-Cacho, Phys. Rev. B **65**, 144409 (2002).
[8]C. L. Bull, D. Gleeson, and K. S. Knight, J. Phys.: Condens. Matter **15**, 4927 (2003).
[9]M. Kitamura, I. Ohkubo, M. Matsunami, K. Horiba, H. Kumigashira, Y. Matsumoto, H. Koinuma, and M. Oshima, Appl. Phys. Lett. **94**, 262503 (2009).
[10]M. P. Singh, K. D. Truong, S. Jandl, and P. Fournier, Phys. Rev. B **79**, 224421 (2009).
[11]Z. Zhang, H. Jian, X. Tang, J. Dai, X. Zhu, and Y. Sun, J. Sol-Gel Sci. Technol. **61**, 224 (2012).
[12]M. N. Iliev, H. Guo, and A. Gupta, Appl. Phys. Lett. **90**, 151914 (2007).
[13]D. Kumar and D. Kaur, J. Alloys Compd. **554**, 277 (2013).
[14]J. Blasco, M. C. Sánchez, J. Pérez-Cacho, J. García, G. Subías, and J. Campo, J. Phys. Chem. Solids **63**, 781 (2002).
[15]J. Blasco, J. García, M. C. Sánchez, J. Campo, G. Subías, and J. Pérez-Cacho, Eur. Phys. J. B **30**, 469 (2002).
[16]K. Devi Chandrasekhar, A. K. Das, C. Mitra, and A. Venimadhav, J. Phys.: Condens. Matter **24**, 495901 (2012).
[17]D. Choudhury, P. Mandal, R. Mathieu, A. Hazarika, S. Rajan, A. Sundaresan, U. V. Waghmare, R. Knut, O. Karis, P. Nordblad, and D. D. Sarma, Phys. Rev. Lett. **108**, 127201 (2012).
[18]K. D. Truong, M. P. Singh, S. Jandl, and P. Fournier, Phys. Rev. B **80**, 134424 (2009).
[19]G. Y. Gao, Y. Wang, Y. Jiang, L. F. Fei, N. Y. Chan, H. L. W. Chan, and W. B. Wu, Thin Solid Films **519**, 6148 (2011).
[20]H. Z. Guo, J. Burgess, E. Ada, S. Street, A. Gupta, M. N. Iliev, A. J. Kellock, C. Magen, M. Varela, and S. J. Pennycook, Phys. Rev. B **77**, 174423 (2008).
[21]M. P. Singh, C. Grygiel, W. C. Sheets, Ph. Boullay, M. Hervieu, W. Prellier, B. Mercey, Ch. Simon, and B. Raveau, Appl. Phys. Lett. **91**, 012503 (2007).
[22]M. Kitamura, I. Ohkubo, M. Kubota, Y. Matsumoto, H. Koinuma, and M. Oshima, Appl. Phys. Lett. **94**, 132506 (2009).
[23]S. Kazan, F. A. Mikailzade, M. Özdemir, B. Aktaş, B. Rameev, and A. Intepe, Appl. Phys. Lett. **97**, 072511 (2010).
[24]Y. L. Tian, W. Zhang, L. Li, Y. Q. Lin, and X. M. Chen, J. Mater. Sci.: Mater Electron. **22**, 116 (2011).
[25]M. Hashisaka, D. Kan, A. Masuno, M. Takano, Y. Shimakawa, and T. Terashima, Appl. Phys. Lett. **89**, 032504 (2006).

[26]Y. Sakurai, I. Ohkubo, Y. Matsumoto, H. Koinuma, and M. Oshima, J. Appl. Phys. **110**, 063913 (2011).
[27]R. J. Zeches, M. D. Rossell, J. X. Zhang, A. J. Hatt, Q. He, C. H. Yang, A. Kumar, A. Melville, C. H. Wang, C. Adamo, G. Sheng, Y. H. Chu, J. F. Ihlefeld, R. Erni, V. Gopalan, C. Ederer, L. Q. Chen, D. G. Schlom, N. A. Spaldin, L. W. Martin, and R. Ramesh, Science **326**, 977 (2009).
[28]R. Takahashi, I. Ohkubo, K. Yamauchi, M. Kitamura, Y. Sakurai, M. Oshima, T. Oguchi, Y. Cho, and M. Lippmaa, Phys. Rev. B **91**, 134107 (2015).
[29]S. R. Spurgeon, Y. Du, T. Droubay, A. Devaraj, X. Sang, P. Longo, P. Yan, P. G. Kotula, V. Shutthanandan, M. E. Bowden, J. M. LeBeau, C. Wang, P. V. Sushko, and S. A. Chambers, Chem. Mater. **28**, 3814 (2016).